Published in final edited form as:
Macromol Biosci. 2010 April 8; 10(4): 393–403. doi:10.1002/mabi.200900294.

Effect of Hydration on Silk Film Material Properties

Brian D. Lawrence[1,3], **Scott Wharram**[2], **Jonathan A. Kluge**[3], **Gary G. Leisk**[4], **Fiorenzo G. Omenetto**[3,5], **Mark I. Rosenblatt**, and **David L. Kaplan**[3]

[1]Department of Biomedical Engineering, Cornell University, 101 Weill Hall, Ithaca, NY 14853

[2]Department of Plastics Engineering, University of Massachusetts at Lowell, 1 University Avenue, Lowell, MA 01854

[3]Department of Biomedical Engineering, Tufts University, Science and Technology Center, 4 Colby St., Medford, MA 02155

[4]Department of Mechanical Engineering, Tufts University, 204 Anderson Hall, 200 College Avenue, Medford, MA 02155

[5]Department of Ophthalmology, Weill Medical College of Cornell University, 1300 York Avenue, New York City, NY 10065

Summary

Effects of hydration on silk fibroin film material properties were investigated for water-annealed and MeOH treated samples. After hydration, thickness increased 60% for MeOH immersed films, while water-annealed samples remained constant. TGA determined MeOH immersed films had an 80% mass loss due to water, while water-annealed had a 40% mass loss. O_2 permeability was greater in MeOH immersed films with Dk values of 10 (10^{-11}·mLO_2·cm)/(cm·s·mmHg), while water-annealed films had Dk values of 2 (10^{-11}·mLO_2·cm)/(cm·s·mmHg). All films showed a decrease in Young's modulus and increased plastic deformation by two orders of magnitude when submerged in saline solution. FTIR revealed water-annealed films increased in β-sheet content with increasing water vapor, while MeOH immersed films did not change.

Keywords

Silk fibroin; films; hydration; oxygen permeability; mechanical properties

Introduction

Webs and cocoons are examples of structures formed from silk proteins, a versatile family of fibrous proteins [1]. Silks have been used by humans for the production of textiles for thousands of years. More recently, silk proteins have been found to offer a versatile range of biomaterial properties that make it desirable for applications in regenerative medicine and tissue engineering [2, 3]. The silk protein fibroin, the primary structural component in *Bombyx mori* cocoons, generates a minimal immune and inflammatory response when implanted within the body, and is degraded by naturally occurring proteolytic enzymes [4–7]. The rate of degradation is directly related to the content of secondary β-sheet crystalline structure present within the bulk material [7–9]. The amount of β-sheet can be modified in silk-based biomaterial structures produced from regenerated silk fibroin through the use of various processing methods [4, 7–12]. Recent efforts have resulted in the formation of films, sponges and hydrogels from regenerated silkworm fibroin [4]. Further efforts are underway to expand the use of fibroin based devices as drug delivery vehicles [13], optical sensors [14, 15], and microfluidic chambers [16, 17].

As the uses for silk fibroin expand it is important to understand how the bulk material properties change when introduced to specific environmental conditions, such as water. Silk fibroin posses both hydrophobic and hydrophilic regions with a block copolymer design [18]. Although the majority of the molecular structure is composed of hydrophobic amino acid regions, the presence of hydrophilic chain ends, as well as intervening hydrophilic regions, allows water to interact with the fibroin protein structure [18]. As a result, water molecules produces a plasticizing affect to alter molecular interactions, potentially impacting the mechanical properties of these materials [19, 20], depending on the thickness, crystallinity and processing history. Only a few studies have focused on how hydration impacts silk material properties since the native fibers are inherently very stable to hydration [19, 21]. Therefore, the current study focused on elucidating the effects of water on bulk material properties of silk fibroin films that were processed using two previously described treatments, methanol (MeOH) solvent immersion [10] and water-annealing [11]. This post-casting of silk solution for film formation processing is required to generate water insoluble films that remain stable when submerged in water, and offering control of secondary structure content.

Previous work has shown that silk films treated with MeOH exhibit almost a 3-fold increase in β-sheet content when compared to water-annealed silk films [22]. Therefore, it is important to understand how silk film material properties change with respect to this change in β-sheet content. For example, this type of information is important for the design of a silk-based devices destined for *in vivo* applications. By better understanding how water influences the properties of silk materials, processing methods can be tailored for selective functions. Furthermore, the organization of protein secondary structure is important for understanding how the presence of solvents, such as water or MeOH, affect film material properties. Therefore, it is important to understand how the content and organization of fibroin secondary structure contributes to changes in material properties [23].

Recent studies have focused on the use of water-annealed silk films for optical devices due to their transparent nature and surface patterning capabilities [14, 15, 22]. These attributes contribute to the versatility of silk biomaterials, as the combination of optical transparency, biodegradability, and superior mechanical strength lend these water-annealed silk films as a suitable material for vision-related medical devices [24]. Specifically, corneal tissue engineering and regeneration provide suitable targets for these silk biomaterials [25]. However, it is important to better understand how the physical properties of these types of silk films are altered within hydrated environments. Therefore, the present study was focused on the characterization of both water-annealed and MeOH submersion treatments in terms of their impact on silk film material swelling, mechanical properties, thermal stability, and oxygen permeability.

Experimental Part

Preparation of Silk Fibroin Solution

As described previously [14, 26] and illustrated in Figure 1, *B. mori* silk cocoons (Institute of Sericulture, Tsukuba, Japan) were cut into fourths and boiled for 45 minutes in 0.02M Na_2CO_3 (Sigma-Aldrich) to extract the glue-like sericin proteins from the structural fibroin proteins. The fibroin extract was then rinsed three times in Milli-Q water, dissolved in 9.3M LiBr solution at room-temperature, and set covered within a 60°C oven for 4 hours. The solution was then dialyzed (MWCO 3,500) in water for 48 hours with 6 water changes at 1, 4, 8, 12, 12 and 12 hour intervals. The dialyzed silk solution was then centrifuged at 13,000 g, and the supernatant was collected and stored at 4°C. The final concentration of aqueous silk solution was 8 wt/vol.% as determined by gravimetric analysis.

Preparation of PDMS Casting Substrates

Flat PDMS substrates of 0.75 mm in thickness, were prepared by casting 38 mL of a 9:1 mixture of silicone potting solution to catalyst (GE Plastics, Inc.) upon 500 cm^2 square petri dishes (Corning Inc., Corning, NY). The solution was then degassed for 2 hours and cured at 60°C for 12 hours. Post curing PDMS circular shapes were punched out with 11 and 30 mm diameter geometries. In addition, PDMS dog-bone geometries were also punched out using the ASTM-D-638-4 standard size sharp edge cutting die, which includes a 3.18 × 9.53 mm neck region for testing. The PDMS substrates were then prepared for silk film casting by washing once with 70% ethanol solution and rinsing three times with dH_sO. PDMS surfaces were used for multiple silk film castings. Between film casting silk residuals were removed using a 9.3M LiBr soaking prior to the washing and rinsing protocol.

Preparation of Silk Films

Three different silk film sample sizes were formed by casting 70 and 400 μL of 8% silk solution onto 11 and 30 mm diameter PDMS rounds, respectively, and casting 400 μL of 8% silk solution onto dog-bone shaped substrates. The volumes for the PDMS round geometries and dog-bone shapes were chosen to optimize the overall casting time and thickness uniformity based on prior casting studies [14, 22]. The films were then covered with a lid that allowed for atmospheric venting. The films were then left to dry overnight at ambient conditions. Once dried, water-annealing processing was performed on one set of silk film samples by placing the dishes on a shelf in a valved container partially filled with water. Next, a 24 mmHg vacuum was pulled within the container, and once vacuum was reached the valve was placed in the closed position. This produces a saturated water vapor environment that induces β-sheet secondary structure formation within the silk film [11]. The films were left within the water vapor environment for a five hour period and then placed into a dH2O bath to await experimentation. Separate sets of silk films were processed using the MeOH solvent immersion, in which the silk films were submerged in 50:50 MeOH to water solution for a minimum of 20 minutes to induce β-sheet formation [10]. Following treatment, the silk film samples were then placed into a dH2O bath to await experimentation. All samples were used for experimentation within a 24 hour period after both casting and processing.

Measurement of Silk Film Thickness

Hydrated and dehydrated dog-bone shaped silk film thicknesses were assessed using 2-photon confocal microscopy. Hydrated samples were incubated for 24 hours within dH_2O at ambient conditions prior to imaging. TPEF/SHG micrographs were acquired for both hydrated and dehydrated silk film samples using a previously described protocol on a Leica DMIRE2 microscope with a TCS SP2 scanner (Wetzlar, Germany) [27]. Images were acquired using a 10× (NA 0.3) dry objective. The excitation light source was a Mai Tai tunable (710–920 nm) titanium sapphire laser emitting 100 fs pulses at 80 MHz (Spectra Physics, Mountain View CA). Samples were placed on glass cover slips (Fischer Scientific, Inc.) and excited at 800 nm. Film thickness was assessed at the center position of the sample neck region. Fluorescence emission spectra were detected from 380 to 700 nm in 100 steps with a 20-nm detector bandwidth. TPEF/SHG images were acquired in the forward direction through a bandpass filter centered at 400 nm (Chroma hq400/20m-2p). Analysis was performed with the Leica Confocal (Wetzlar, Germany) and ImageJ software (NIH, Bethesda, MD).

Sample cross-sectional thickness images were obtained using the “Section” function within the Leica Confocal Software. These images were then exported to ImageJ for analysis. Film thickness (δ) was assessed by measuring the z-y or z-x planes of each image that was generated from the collected TPEF/SHG signal z-stack profile. Film thickness was measured

by assessing the cross-sectional region of each z-stack image using the “Plot Profile” function within the Image-J software package. The “Plot Profile” function outputs the average signal intensity for each pixel line versus the distance along the selected region of the image. Therefore, silk film thickness can be determined by the position of TPEF/SHG signal intensity distribution at a given threshold level, which can be validated against other imaging modalities, such as scanning electron microscopy (SEM), as described below.

The calculated threshold for signal intensity that indicates silk film presence was validated by comparing against a previously described SEM imaging methodology for assessing the sample cross-sectional area [14, 22]. Dog-bone film samples from each processing condition were randomly selected from each sample population and prepared for SEM imaging. Samples were prepared for SEM by flash freezing in liquid nitrogen and cracking the film with a razor blade at the center of the dog-bone neck region. The samples were then adhered to aluminum platforms using conductive tape (Electron Microscopy Sciences, Hatfield, PA), and then sputter coated with 40 nm of gold using a Polaron SC502 Sputter Coater (Fisons, VG Microtech, East Sussex, England). Silk film cross-sectional thickness of each image was analyzed using ImageJ software (NIH, Bethesda, MD). Film thickness measured by SEM was then compared to the collected TPEF/SHG signal distribution. Silk film sample thickness was found to be most similar between both imaging modalities above 80% of the maximum TPEF/SHG signal intensity for each compiled sample z-stack. Silk film thickness swelling ratios (Q) were then calculated using the expression:

$$Q=\frac{\delta_H}{\delta_D} \tag{1}$$

where Q is the silk film thickness swelling ratio, δ_H is the hydrated film thickness, and δ_D is the dehydrated film thickness. Sample thickness measurements and Q values were statistically assessed with the Student t-test for means in both the validation study and comparing differences between hydrated and dehydrated film thicknesses.

Uniaxial Tensile Testing of Hydrated Silk Films

Tensile tests were performed on an Instron 3366 testing frame equipped with a 100N capacity load cell and Biopuls™ pneumatic clamps. Dog-bone shaped silk film samples were hydrated in 0.1M phosphate buffered saline (PBS) for 30 minutes to equilibrate prior to testing. Test samples were submerged into the Biopuls™ temperature-controlled testing container filled with PBS solution (37±0.3°C) for 5 minutes prior to and for the duration of testing. A displacement control mode was used, with a crosshead displacement rate of 10 $mm \cdot min^{-1}$. The measured width of the gauge region of the PDMS slat was multiplied by the specimen thickness (measured by two-photon confocal microscopy) in order to convert load data to tensile stress values. The corresponding strain was measured using an Instron Video Extensometer that tracked the position of 2 painted dots placed 1 cm apart. The initial “linear elastic modulus”, yield stress, elongation to failure, and ultimate tensile strength were calculated from stress/strain plots. The initial “linear elastic modulus” was calculated by using a least-squares’ (LS) fitting between 0.05N load and 5% strain past this initial load point. The yield strength was determined by offsetting the LS line by 2% strain and finding the data intercept. Ultimate tensile strength (UTS) was determined as the highest stress value attained during the test. The elongation to failure was determined as the last data point before a >10% decrease in load (failure strain minus the strain corresponding to 0.05 N load noted earlier). Sample sets were statistically analyzed by using a Student t-test analysis of means.

TGA

The water content in both hydrated and dehydrated silk films were estimated using thermal gravimetric analysis (TGA). TGA has been used to characterize water content within silk fibroin films [20, 21]. TGA measurements were performed using a TA 500Q system (TA Instruments, New Castle, DE). Prior to loading, 11 mm round silk film samples were either hydrated in dH2O for 24 hours at ambient conditions, or stored in the open ambient environment for 24 hours. Hydrated samples were wiped along the sides of their plastic storage vessels to remove non-absorbed surface water, and immediately loaded into the enclosed TGA oven. All samples were heated to 600°C at 10°C/min under an inert nitrogen atmosphere with a flow rate of 40 mL/min. Water mass loss was assessed by observing the percent of initial weight located at the plateau region of the TGA profiles. Thermal stability of the silk film samples was assessed through 1st derivative peak location from the collected TGA mass loss profiles for both hydrated and dehydrated samples of each processing condition. Such analysis provides insight into the affects of water absorption on the thermal stability of silk films, and may provide insight into how the presence of secondary structures, such as β-sheet content, affect water absorption. Specifically, the position of the 1st derivative(s) of a TGA profile assesses the change in mass loss during the heating cycle due to material phase changes at a specific temperature, such as water evaporation and material degradation thresholds. Thus, changes in β-sheet content may affect the temperatures at which these phase transitions take place [28]. Data were normalized to initial mass values for each sample. Statistical analysis between groups was assessed using Student t-tests.

O_2 Permeability

Oxygen permeation studies were conducted using the Illinois 8001 Oxygen Permeation Analyzer (Illinois Instruments, Johnsburg, Illinois; ASTM 3985-05). In the first study, circular 11 mm diameter silk films were saturated with dH_2O and evaluated at 37°C and 80% relative humidity (RH) over 15 minute test intervals for a total of 135 minutes. Dry samples were then tested at 37°C and 50% RH using the same time intervals. Oxygen gas transmissibility rates (O_2GTR) were recorded. Sample thickness measurements were recorded for each silk film employing the Ono Sokki EG-225F Digital Indicator (AA821 Radius Point; 25g force). Oxygen permeability (PO_2) rates were calculated for each silk model in accordance with ASTM 3985-05 as follows:

$$PO_2 = \frac{O^2GTR}{p} \tag{2}$$

where O^2GTR is the oxygen transmissibility rate ($mLO_2/(cm^2 \cdot day)$), and *p* is the partial pressure of oxygen and is the mol fraction of oxygen multiplied by 1 atm of pressure. These conditions where assumed to be taken as 1 cm^3(STP) is 44.62 μmol, 1 atm is 759.81 mmHg, and one day is $86.4 \cdot 10^6$ s.

The acquired O_2GTR values were then converted to thickness dependent oxygen permeability coefficients (Dk) to provide normalized measurements to enable comparison of oxygen permeability across different treatment conditions. The unit of permeance is then given as $mLO_2/(cm^2 \cdot s \cdot mmHg)$. Oxygen permeability coefficients (Dk) for each sample were calculated by:

$$Dk = PO_2 \cdot t \tag{3}$$

where t is thickness of the homogenous silk material in cm. The units of Dk is taken to be (mLO_2·cm)/(cm·s·mmHg).

FTIR Spectroscopy

Silk film secondary structural analysis was measured using an FTIR spectrometer (Vertex80V, Bruker Optics, Inc., Germany). Spectral scans were obtained using dried samples from each processing condition. For each sample a measurement of 66 scans was collected at a resolution of 4 cm^{-1}, which was acquired over a wavenumber range of 400–4000 cm^{-1}. Spectral manipulations were performed with OPUS (version 6.0 software, Bruker Optics, Inc.). Quantification of silk secondary structure was based on analyzing the amide I region (1600–1700 cm^{-1}) [29]. Background absorption due to water was subtracted from the sample spectra to obtain a flat recording in the range of 1750–2000 cm^{-1} [30]. The amide I region (1580–1710 cm^{-1}) was selected from the entire spectrum, and a linear baseline was applied to the spectrum.

Results and Discussion

Silk Film Thickness Analysis

When MeOH processed or water-annealed silk films are incubated within a water bath for an extended period of time (> 2 hrs) the films are notably larger in size, which is most likely due to water absorption creating changes in the protein secondary structure. The larger macroscopic geometrical changes in width and height are straightforward to measure with a caliper device; however the micron sized thickness measurements prove more difficult to quantify. Previous studies have evaluated silk film cross-sectional thickness using scanning electron microscopy (SEM) [11, 14]. However, under SEM imaging conditions samples are dry and under high vacuum. Therefore, a representative cross-sectional thickness cannot be achieved for a silk film in the hydrated state, which would be more applicable to physiological conditions. 2-Photon Excited Fluorescence and Second Harmonic Generation (TPEF/SHG) has been used to monitor silk film material features under hydrated conditions [27, 31]. In addition, because this imaging method is non-invasive it allows for the same samples to be used for subsequent testing, unlike the case with SEM. Therefore, TPEF/SHG confocal imaging was used to measure the thickness of the dog-bone silk film samples. Z-stack images were generated from the collected TPEF/SHG signal (Figure 1a), and used to assess the cross-sectional region of both hydrated and dehydrated film samples produced using water-annealing or MeOH treatments. The thickness measurements were used to calculate silk film thickness swelling ratios (Q), and later used to assess mechanical properties.

The center of the neck region for each sample was used for imaging. Film thickness was determined by measuring the distance between the 80% initial maximum positions from collected TPEF/SHG signal distribution curves generated from 2-photon confocal microscopy z-stack images (Figure 1b). This signal threshold was validated by comparing the TPEF/SHG signal distribution distances to SEM cross-sectional measurements for randomly selected dog-bone silk film samples from both MeOH immersion and water-annealed treatments (Figure 1c). Randomly selected dehydrated sample thicknesses from both processing conditions were obtained from both imaging modalities. The results of this experiment indicate that TPEF/SHG analysis provides the same thickness measurements as standard SEM analysis for dry sample thicknesses, providing validation for the use of the 2-photon excited imaging modality for film thickness measurement (Figure 1d). The results also suggest that the hydration level in the films is low under dehydrated conditions at ambient conditions, as otherwise, significant artifacts would be anticipated during SEM analysis, which was not the case.

Silk film thickness measurements and swelling ratios (Q) were collected for both hydrated and dehydrated states using the TPEF/SHG signal distribution (Table 1). Silk films treated by MeOH immersion showed a statistical increase in thickness in the hydrated state when compared to the dehydrated state (Figure 2a). However, water-annealed silk films did not show significant differences in thickness between hydrated and dehydrated states (Figure 2a).

These results indicate that there is a difference in silk film swelling due to the hydration state and treatment conditions. A statistically significant increase in Q for MeOH immersed silk film samples was found when compared to water-annealed samples (Figure 2b). These results demonstrate that silk film samples treated by MeOH immersion have a nearly 60% increase in film thickness when placed in a hydrated environment. Previously, it has been demonstrated that water-annealed film samples had a nearly 3 fold decrease in β-sheet content when compared to MeOH treated films [22]. Therefore, increasing β-sheet content by MeOH immersion is directly related to increased silk film thickness after hydration. These results suggest greater water absorption is occurring in the MeOH immersed films when compared to the water-annealed samples. Thus, these results infer that β-sheet content and secondary structure organization play a significant role in silk film water absorption properties.

Silk Film Mechanical Properties

Silk films with dog-bone geometries were submerged in 0.1M PBS solution and heated to 37°C before testing to better represent physiological conditions during uniaxial mechanical testing. All samples were then pulled to failure at a 10 mm/min cross-head rate. Failure was absolute for every sample and was confined to the neck region of the dog-bone geometry. Representative stress-strain curves for both water-annealed and MeOH immersed films are shown in Figure 3. The two processing conditions exhibited similar force vs. axial strain profiles, which is indicative that both materials possess similar mechanical properties when tested in the hydrated testing state. This result is somewhat unexpected as it has been previously demonstrated that MeOH immersed silk films have greater β-sheet content than water-annealed films, and this increased β-sheet content has been thought to result in enhanced stiffness in the dry testing states [11, 32]. However, hydrated films exhibit over an order magnitude decrease in tensile strength whem compared to dehydrated samples for both processing conditions [11]. Therefore, this result indicates that the presence of water had a significant effect on silk film mechanical properties regardless of β-sheet content.

Both processing conditions resulted in similar elongation to failure values (Table 2), in which both sets of samples failed at around 140% strain. This was approximately two orders of magnitude increase in elongation to failure when compared to dehydrated samples from both processing conditions [11]. These results indicate that the silk films exhibit an increase in plastic deformation within a hydrated environment when compared to their dry states. However, it is uncertain if there is an increase in elastic deformation for the hydrated state. These results further support the notion that water acts as a plasticizer between the fibroin proteins forming the silk film [20].

A significant increase ($p < 0.05$, $n = 4$) in average silk film cross-sectional area was found for MeOH immersed samples when compared to water-annealed samples. These results infer that silk film material failure is primarily a function of fibroin chain breaks after extended plastic deformation, and material failure appears to be less a function of water absorption. A three-fold increase in the standard deviation was found for MeOH immersed samples when compared to water-annealed samples. This increase in standard deviation is likely due to greater silk film thickness non-uniformity caused by increased water-absorption, which most likely correspond to the overall degree of molecular organization

within and between the amorphous and crystalline domains of the film. More specifically, the increased β-sheet content within MeOH treated films as compared to water-annealed films appears to be an indicator for the degree of film thickness swelling. Thus, in the dry testing state the presence of greater β-sheet content corresponds with enhanced silk film stiffness, while in the hydrated testing state increased β-sheet content corresponds with increased water absorption, which has a greater affect on increasing material ductility as opposed to promoting enhanced material strength.

Water Absorption and Thermal Stability Determined by TGA

The differences observed in silk film thickness between the water-annealed and MeOH immersed samples show that greater water absorption occurred in the MeOH immersed samples. Thermal gravimetric analysis (TGA) was performed on both hydrated and dehydrated silk film samples to determine how much water absorption occurred and the affect on material properties (Figure 4ab). TGA profiles for dehydrated samples did not significantly differ between the two processing conditions, and mass loss due to water was not found to be statistically different. However, a difference in TGA profiles was noted between the two processing groups for the hydrated samples. Hydrated water-annealed films exhibited a statistically significant increase ($p<0.005$, $n=3$) in mass loss of water when compared to the hydrated methanol treated films. These results indicate that MeOH immersed films absorb more water comparatively to water-annealed films in the hydrated state. These results correspond with the above silk film thickness measurements indicating an increase in thickness for hydrated MeOH films when compared to their dehydrated state.

The results of TGA 1st derivative analysis are summarized in Table 4. The 1st derivative plotted profiles demonstrated significant differences in both plot profiles and peak location between the hydrated and dehydrated silk film samples (Figure 4c–f). For dehydrated silk film samples there was a statistically significant ($p<0.01$, $n=3$) shift to a higher material degradation temperature for methanol treated samples when compare to water-annealed films (Figure 4cd). This observation has been previously shown in the literature and has been suggested to be related to greater β-sheet secondary structure formation within the film bulk material of MeOH treated films [20, 28]. In contrast, the location of the 1st derivative position corresponding to the material degradation phase shift, the second small peak, did not change between hydrated samples of different processing conditions (Figure 4df). In addition, hydrated samples exhibited a large 1st peak, which likely corresponding to water loss due to evaporation. This first peak was shifted to a higher temperature for methanol treated samples and did not appear for two of the three water-annealed samples. This indicated that more energy was required to evaporate absorbed water from the MeOH immersed silk films when compared to water-annealed samples. Additionally, the larger size of the first peak for MeOH immersed samples indicated a greater phase shift when compared to water-annealed samples, which corresponds to a greater release of absorbed water.

Silk Film O_2 Permeability and FTIR Analysis

Adequate oxygen diffusion throughout a scaffold construct is a requirement for the maintenance of living cells, especially in relation to a 3D environment. In addition, oxygen permeability can provide useful insight into silk protein secondary structure organization post processing. Therefore, the impact of β-sheet crystalline content on both oxygen permeability and secondary structure organization within the films was assessed. The values for silk film thickness, O_2GTR, Dk, and time to steady state permeability for various conditions are listed in Table 5.

Dk was plotted versus time for both RH conditions for each silk film treatment method (Figure 5). Dk increased over time for both silk film processing conditions at 80% RH, while samples tested in 50% RH conditions exhibited a decrease in Dk over time. MeOH treated silk films exhibited increased oxygen permeability over time for both RH conditions when compared to water-annealed samples. Furthermore, MeOH treated samples exhibited a persistent change in Dk values over time for both RH conditions over the entire 135 minute testing period. These results indicate that the MeOH treated films go through a greater change in secondary structure. However, water-annealed samples reached rapid stabilization for both RH conditions, at 50 and 65 minutes on average for both 50% and 80% RH conditions, respectively. These results indicate that water-annealed silk film secondary structure reaches stabilization at a more rapid rate. Furthermore, the extended length of Dk stabilization exhibited by MeOH treated silk films corresponds to their greater water absorption properties. As a result the MeOH treated films have greater Dk instability profiles when compared to water-annealed samples due to their increased hydrated state which impacts the silk film secondary structure and ultimately the oxygen permeability rates through this structure.

Dk values for all samples were found to increase over the first 15 minutes of experimentation, while after 135 minutes the Dk values decreased for both treatment methods at 50% RH conditions (Table 5). Additionally, a significant difference ($p < 0.05$, $n = 3$) was shown between water-annealed and MeOH treated films at 80% RH for both time points, indicating that the selected film processing method changes the oxygen permeability properties for silk films in hydrated conditions. Similar results were shown for films run at 50% RH conditions in which MeOH treated films showed a significantly higher Dk value for both time points. The above results infer that MeOH treatment is producing a difference in protein secondary structure within the silk film bulk region that is more permeable to oxygen than the structure formed through water-anneal processing.

These results compared favorably with previously published data for MeOH treated silk films in the hydrated state [33, 34]. However, no previous O_2 permeability studies have been undertaken for water-annealed silk films. It has been previously shown that water-annealed silk film secondary structure is more amorphous when compared to MeOH treated films [22]. The difference in permeability rates between the more crystalline MeOH films and the more amorphous water-annealed films may be attributed to the packing structure of the fibroin protein chains. Amorphous chain movement will be more inhibited when in close proximity to crystalline regions within the bulk polymer structure [34]. Previously it has been suggested that water-annealed films exhibit a tighter packing structure within the bulk region then MeOH treated films. This is thought to be due to the relatively slow rate of secondary structure formation during the water-annealing process (< 4 hours) as compared to MeOH treated films in which the β-sheet structure is formed at a relatively rapid rate (< 20 minutes) [11, 22, 35, 36]. The rapid β-sheet structure induced through MeOH treatment may produce a more disorganized structure between the crystalline and amorphous regions, which enables greater water absorption and increased chain movement within the bulk structure, and thus greater oxygen permeability. As a result there is an increase in Dk for MeOH treated films when compared to water-annealed samples.

Further FTIR analysis of silk film secondary structure pre- and post-testing for O_2 permeability provides further evidence that water-annealed films exhibit a tighter packing order when compared to MeOH treated films. After exposure to different humidity conditions (50% and 80% RH) during O_2 permeability testing, water-annealed films were found to have increasing amounts of β-sheet content as the amount of water vapor flowing through the sample increased (Figure 6). A distinct shift of the random coil peak of 1645 cm^{-1} to the distinctive β-sheet peak located around 1620 cm^{-1} can be observed. In addition,

a slight increasing β-sheet peak can also be seen around 1700 cm^{-1} in the FTIR spectra [22, 28].

However, MeOH treated samples for both pretested and tested samples indicated no change in peak signatures, thus indicating that the β-sheet crystalline structure is fully set before water vapor exposure (Figure 6). These results indicate that the water-annealed bulk protein chains are continuing to undergo structural rearrangement upon exposure to varying amounts of water-vapor which then settles over time. These results correspond with the above O_2 permeability results in which the water-annealed films form a tighter barrier to O_2 when compared to MeOH treated samples. This is likely due to the water-anneal film's bulk secondary structure rearranging to a more densely packed β-sheet crystalline conformation, as opposed to a more randomly ordered β-sheet crystalline matrix formed for MeOH treated films.

Conclusions

This study demonstrates that silk film hydration influences material property outcomes dependent on the choice of processing technique employed. The organization of silk film secondary structure of both amorphous and crystalline regions greatly influences water absorption, and hence dictates material properties such as swelling ratio, mechanical strength, and oxygen permeability. It was determined that MeOH treated films exhibited a less ordered secondary structure arrangement when compared to water-annealed films. As a result, the less ordered MeOH treated films possessed a greater capacity to absorb water and reach higher rates of oxygen permeability. Although one of the most intriguing aspects of silk is the potential to dial-in crystalline content similar to an engineering polymer, this control has to be managed through controlled water content in order to generate materials with consistent material properties. Further work will have to be undertaken to understand how controlled hydration input can be used to produce desired material properties. In summary, the breadth of silk utility is directly related to its varying secondary structures, which in turn are largely dictated by hydration.

Acknowledgments

The authors thank the NIH P41 Tissue Engineering Resource Center for support for this work. In addition, this material is based upon work supported in part by the U.S. Army Research Laboratory and the U.S. Army Research Office under contract number W911NF-07-1-0618 and by the DARPA-DSO.

References

1. Shear WA, Palmer JM, Coddington JA, Bonamo PM. Science. 1989; 246:479. [PubMed: 17788699]
2. Altman GH, Diaz F, Jakuba C, Calabro T, Horan RL, Chen J, Lu H, Richmond J, Kaplan DL. Biomaterials. 2003; 24:401. [PubMed: 12423595]
3. Altman GH, Horan RL, Lu HH, Moreau J, Martin I, Richmond JC, Kaplan DL. Biomaterials. 2002; 23:4131. [PubMed: 12182315]
4. Vepari C, Kaplan DL. Progress in Polymer Science (Oxford). 2007; 32:991.
5. Panilaitis B, Altman GH, Chen J, Jin HJ, Karageorgiou V, Kaplan DL. Biomaterials. 2003; 24:3079. [PubMed: 12895580]
6. Meinel L, Hofmann S, Karageorgiou V, Kirker-Head C, McCool J, Gronwicz G, Zichner L, Langer R, Vunjak-Novakavic G, Kaplan DL. Biomaterials. 2005; 26:147. [PubMed: 15207461]
7. Wang Y, Rudym DD, Walsh A, Abrahamsen L, Kim HJ, Kim HS, Kirker-Head C, Kaplan DL. Biomaterials. 2008; 29:3415. [PubMed: 18502501]
8. Arai T, Freddi G, Innocenti R, Tsukada M. Journal of Applied Polymer Science. 2004; 91:2383.
9. Horan RL, Antle K, Collette AL, Wang Y, Huang J, Moreau JE, Volloch V, Kaplan DL, Altman GH. Biomaterials. 2005; 26:3385. [PubMed: 15621227]

10. Tsukada M, Gotoh Y, Nagura M, Minoura N, Kasai N, Freddi G. Journal of Polymer Science, Part B: Polymer Physics. 1994; 32:961.
11. Jin HJ, Park J, Karageorgiou V, Kim UJ, Valluzzi R, Cebe P, Kaplan DL. Advanced Functional Materials. 2005; 15:1241.
12. Kim UJ, Park J, Joo Kim H, Wada M, Kaplan DL. Biomaterials. 2005; 26:2775. [PubMed: 15585282]
13. Hofmann S, Wong Po Foo CT, Rossetti F, Textor M, Vunjak-Novakovic G, Kaplan DL, Merkle HP, Meinel L. Journal of Controlled Release. 2006; 111:219. [PubMed: 16458987]
14. Lawrence BD, Cronin-Golomb M, Georgakoudi I, Kaplan DL, Omenetto FG. Biomacromolecules. 2008; 9:1214. [PubMed: 18370418]
15. Omenetto FG, Kaplan DL. Nature Photonics. 2008; 2:641.
16. Bettinger CJ, Cyr KM, Matsumoto A, Langer R, Borenstein JT, Kaplan DL. Advanced Materials. 2007; 19:2847. [PubMed: 19424448]
17. Lawrence, B.; Perry, H.; Domachuk, P.; Cronin-Golomb, M.; Georgakoudi, I.; Kaplan, DL.; Omenetto, FG. Silk fibroin-based active optofluidics. 2008; Conference on Quantum Electronics and Laser Science Conference on Lasers and Electro-Optics; CLEO/QELS; 2008.
18. Jin HJ, Kaplan DL. Nature. 2003; 424:1057. [PubMed: 12944968]
19. Hu X, Kaplan D, Cebe P. Thermochimica Acta. 2007; 461:137.
20. Motta A, Fambri L, Migliaresi C. Macromolecular Chemistry and Physics. 2002; 203:1658.
21. Agarwal K, Hoagland DA, Farris RJ. Journal of Applied Polymer Science. 1997; 63:401.
22. Lawrence BD, Omenetto F, Chui K, Kaplan DL. Journal of Materials Science. 2008; 43:6967.
23. Shao Z, Vollrath F. Nature. 2002; 418:741. [PubMed: 12181556]
24. Lawrence BD, Marchant JK, Pindrus MA, Omenetto FG, Kaplan DL. Biomaterials. 2009; 30:1299. [PubMed: 19059642]
25. Chirila TV, Barnard Z, Zainuddin, Harkin DG, Schwab IR, Hirst LW. Tissue Engineering Part A. 2008; 14:1203. [PubMed: 18380593]
26. Jin HJ, Park J, Valluzzi R, Cebe P, Kaplan DL. Biomacromolecules. 2004; 5:711. [PubMed: 15132651]
27. Rice WL, Firdous S, Gupta S, Hunter M, Foo CWP, Wang Y, Kim HJ, Kaplan DL, Georgakoudi I. Biomaterials. 2008; 29:2015. [PubMed: 18291520]
28. Hu X, Kaplan DL, Cebe P. Macromolecules. 2006; 39:6161.
29. Arrondo JLR, Muga A, Castresana J, Gon?i FM. Progress in Biophysics and Molecular Biology. 1993; 59:23. [PubMed: 8419985]
30. Dong A, Huang P, Caughey WS. Biochemistry. 1990; 29:3303. [PubMed: 2159334]
31. Zoumi A, Yeh A, Tromberg BJ. Proceedings of the National Academy of Sciences of the United States of America. 2002; 99:11014. [PubMed: 12177437]
32. Lawrence BD, Omenetto F, Chui K, Kaplan DL. Journal of Materials Science. 2008 In press.
33. Minoura N, Tsukada M, Nagura M. Biomaterials. 1990; 11:430. [PubMed: 2207234]
34. Minoura N, Tsukada M, Nagura M. Polymer. 1990; 31:265.
35. Chen X, Shao Z, Marinkovic NS, Miller LM, Zhou P, Chance MR. Biophysical Chemistry. 2001; 89:25. [PubMed: 11246743]
36. Chen X, Shao Z, Knight DP, Vollrath F. Proteins: Structure, Function and Genetics. 2007; 68:223.

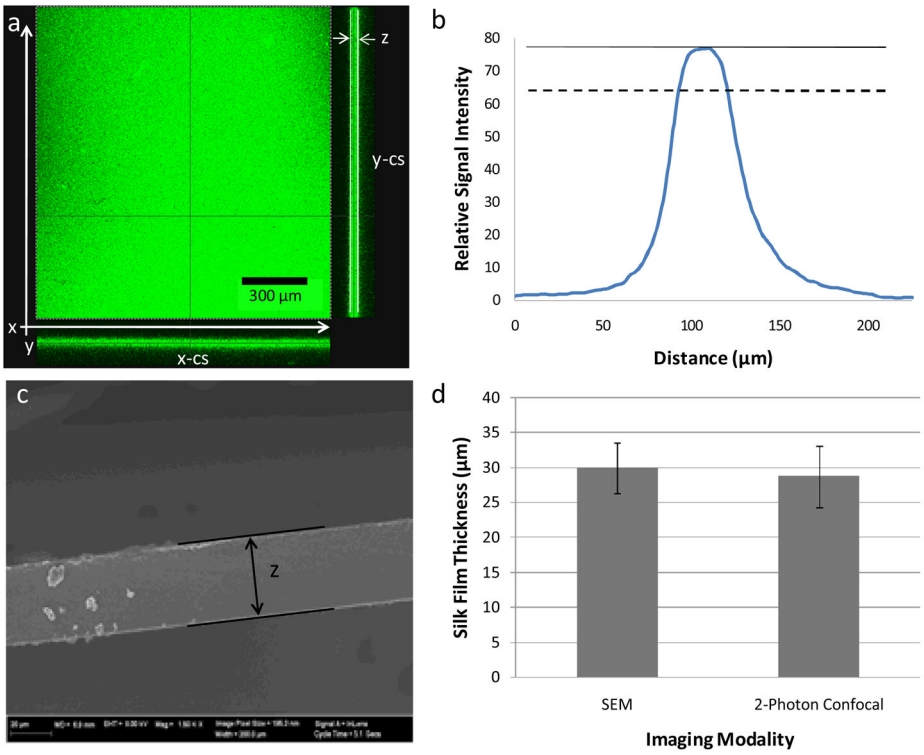

Figure 1.

(a) Representative z-stack images of both end face and cross-sectional views generated from the collected TPEF/SHG signal using 2-photon confocal microscopy. Both x-z (x-cs) and y-z (y-cs) cross sectional images are shown at the bottom and right of the end face view, respectively. (b) Representative signal distribution obtained from z-stack images that illustrate the maximal intensity (solid line) and the signal cutoff at 80% maximal signal (dashed line) (c) Representative SEM image of silk film sample cross-section. (d) Results from validation study showing similar film thickness values achieved from both imaging modalities for randomly selected samples from both treatment conditions (n = 4, error bars = SD).

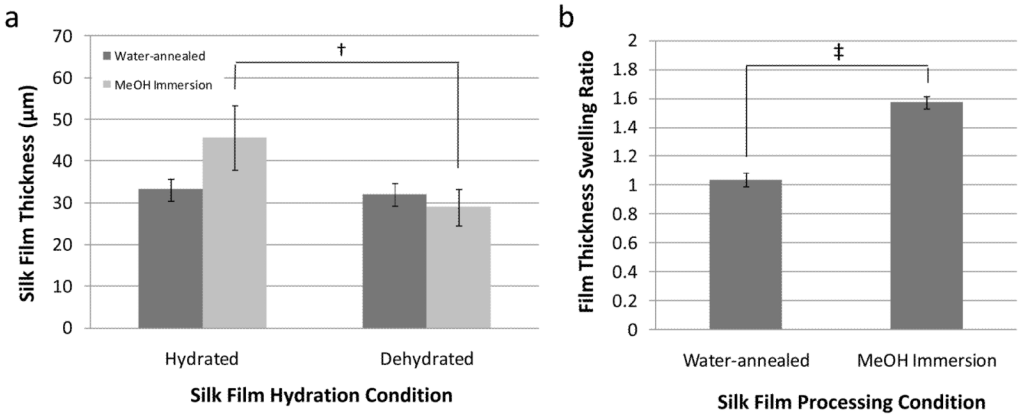

Figure 2.

(a) Silk film thicknesses for dog-bone film geometries measured from 2-photon confocal microscopy for both hydrated and dehydrated conditions. Hydrated MeOH immersion treated films had a statistically significant increase in thickness when compared to their dehydrated state († indicates $p < 0.05$, $n = 3$, error bars = SD). Water annealed films showed no significant change in thickness between hydrated and dehydrated states. (b) The silk film thickness swelling ratio for MeOH immersion treated films was significantly greater then water-annealed film samples (‡ indicates $p < 0.001$, $n = 3$, error bars = SD).

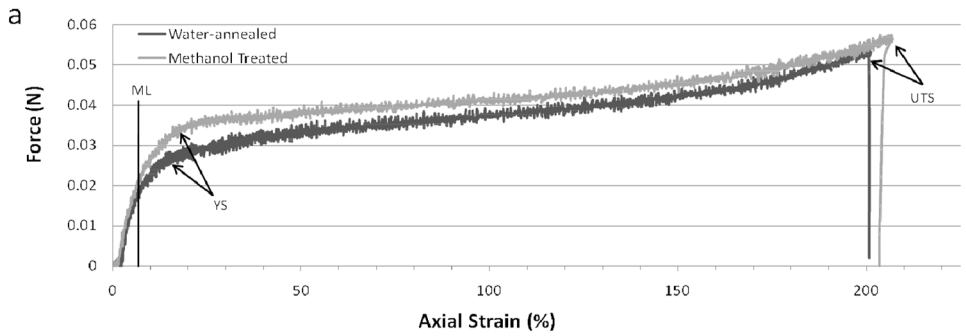

Figure 3.
Representative stress versus strain curves for water-annealed (blue) and MeOH (red) treated silk films showing the modulus line (ML), yield strength (YS), and ultimate tensile strength (UTS).

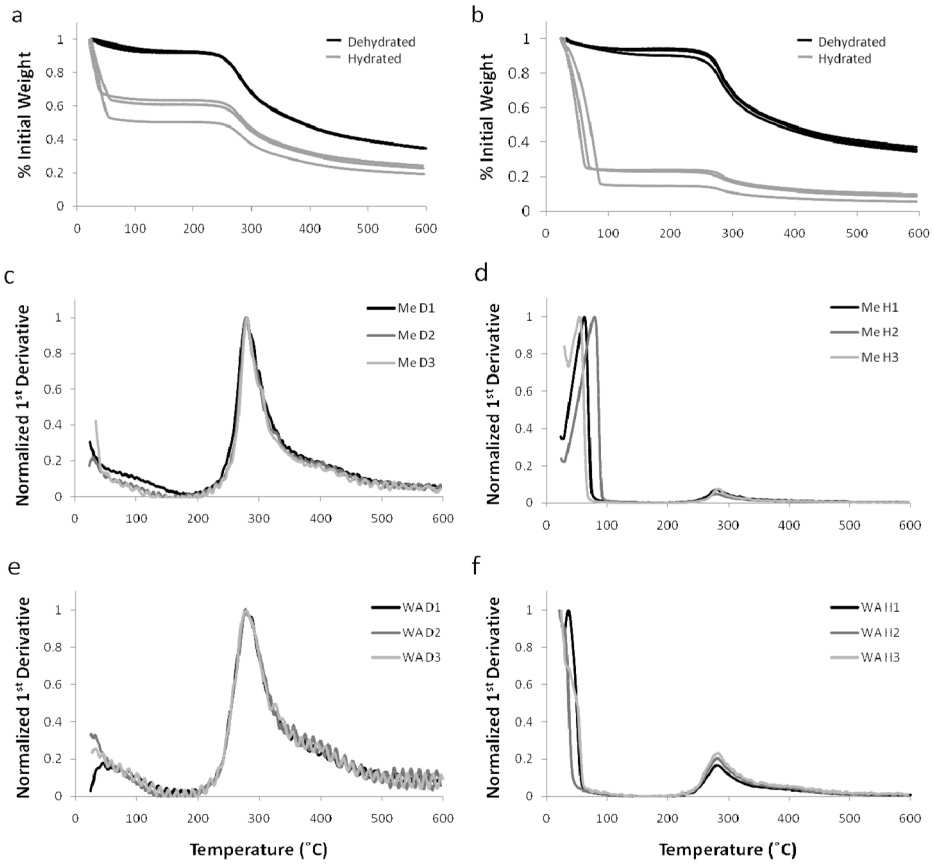

Figure 4.

TGA mass loss profiles with respect to increasing temperature for hydrated (H1-3) and dehydrated (D1-3) silk fibroin films processed for (a) water-annealed and (b) MeOH immersed treatment methods. Normalized TGA 1st derivative profiles for (c, d) methanol treated (Me) and (e, f) water-annealed (WA) films in the hydrated (H) and dehydrated (D) state, respectively. Primary peaks were found for hydrated samples that correspond to water loss due to evaporation in addition to the secondary peaks indicating material degradation.

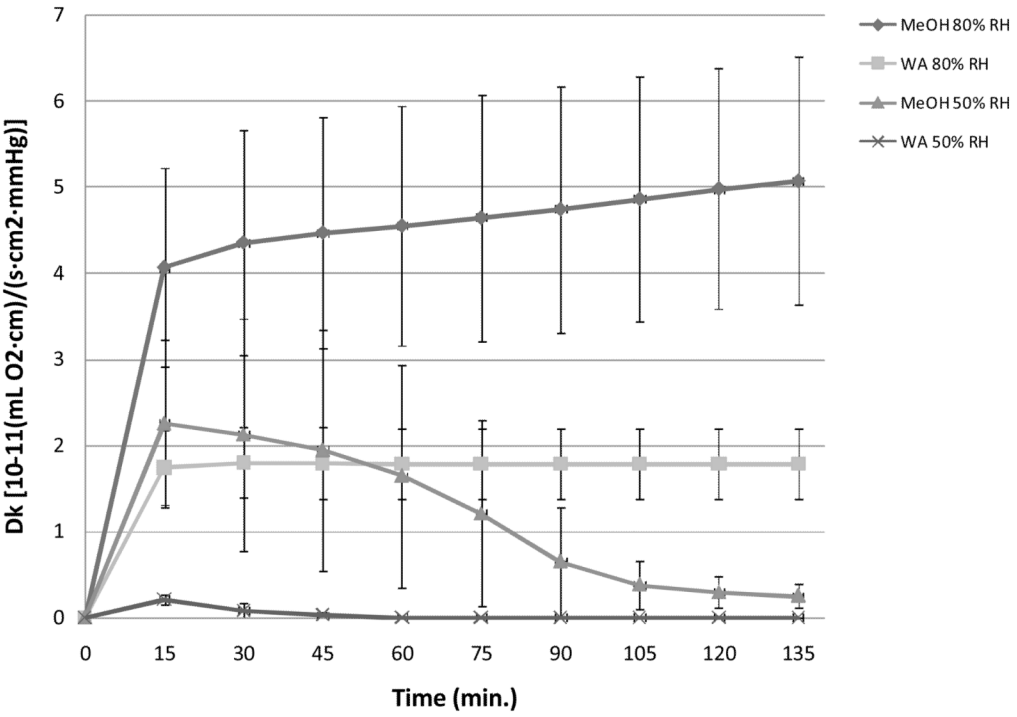

Figure 5.

Oxygen permeability coefficient (Dk) profiles versus time for both MeOH treated and water-annealed (WA) silk film samples at 50% and 80% relative humidity (RH) conditions (n = 3, error bars = SD).

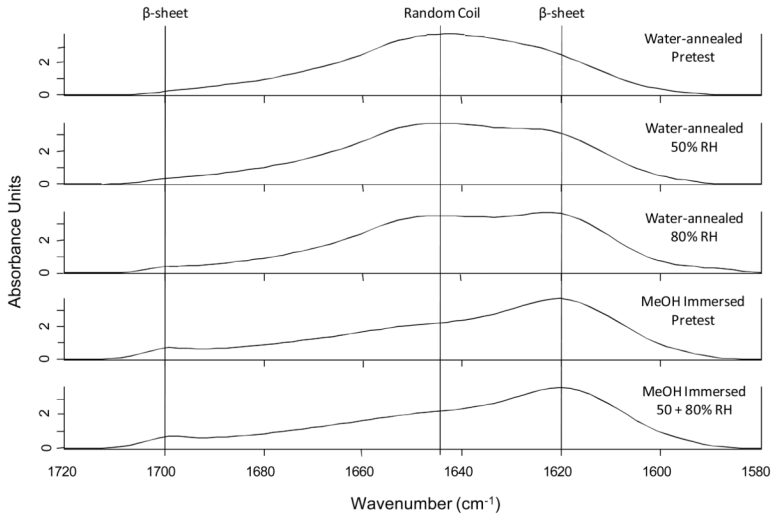

Figure 6.

FTIR spectrum of silk film samples before and after exposure to varying amounts of water-vapor. Distinct spectral signatures for both random coil and β-sheet structures are shown, and sample type is given at right.

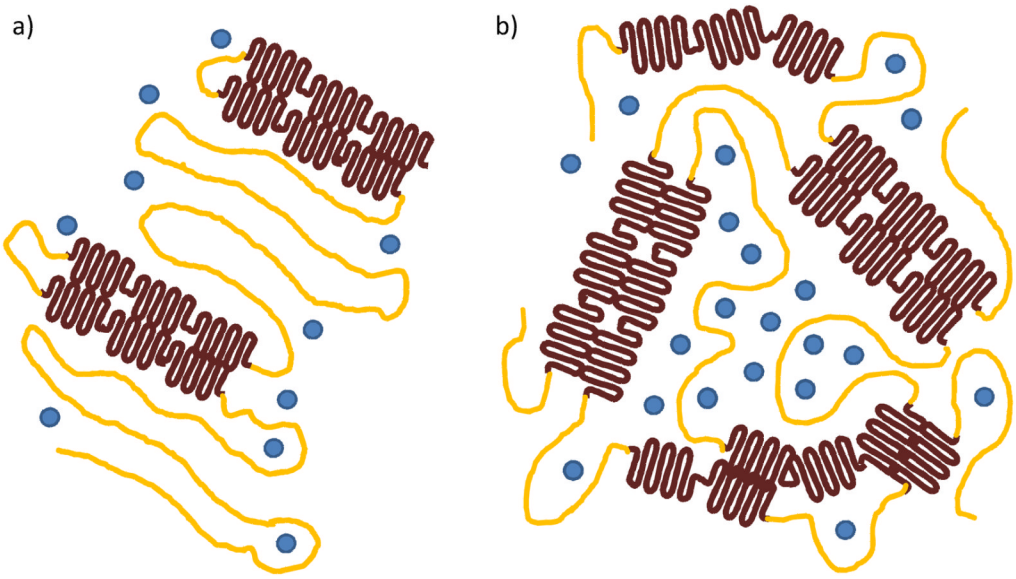

Figure 7.
Schematic representation of silk film secondary structure organization for amorphous (yellow), β-sheet crystalline regions (brown), and water molecules (blue) for both water-annealed (a) and MeOH immersed processing methods. Water-annealing produces less crystalline content but increased ordering of overall secondary structure, while the MeOH treatment produces greater β-sheet content with a highly disordered packing structure. As a result channel-like regions are produced in the amorphous spacing within the MeOH treated films that increases water absorption and oxygen permeability when compared to water-annealed films.

Table 1

Silk film sample thickness (δ_H, δ_D) and swelling ratios (Q) obtained from 2-photon confocal imaging for both hydrated and dehydrated processing conditions.

Sample	Water-annealed			MeOH Immersion		
	δ_H	δ_D	Q	δ_H	δ_D	Q
1	31.0	31.0	1.0	48.0	31.0	1.5
2	36.0	35.0	1.0	37.0	24.0	1..5
3	32.5	30.0	1.1	52.0	32.0	1.6
Avg	**33.2**	**32.0**	**1.0**	**45.7**	**29.0**	**1.6**
St Dev	**2.6**	**2.6**	**0.1**	**7.8**	**4.4**	**0.1**

Macromol Biosci. Author manuscript; available in PMC 2011 July 25.

Table 2

Silk film mechanical properties for different processing conditions.

Water-annealed Samples						
Sample	**Film Thickness (um)**	**Cross-Sect Area (mm^2)**	**Young's Modulus (MPa)**	**Yield Strength (MPa)**	**Ultimate Tensile Strength (MPa)**	**Elongation to Failure (%)**
1	36	0.11	23.02	1.93	3.48	131
2	35	0.11	23.48	2.10	4.69	197
3	37	0.12	20.32	2.08	3.26	138
4	31	0.10	21.05	1.91	3.01	80
Avg	**35**	**0.11**	**21.97**	**2.00**	**3.61**	**136**
St Dev	**3**	**0.01**	**1.52**	**0.10**	**0.75**	**48**

MeOH Immersed Samples						
Sample	**Film Thickness (um)**	**Cross-Sect Area (mm^2)**	**Young's Modulus (MPa)**	**Yield Strength (MPa)**	**Ultimate Tensile Strength (MPa)**	**Elongation to Failure (%)**
1	63	0.20	21.89	1.77	3.74	159
2	48	0.15	9.24	2.53	3.19	135
3	41	0.13	25.51	2.17	3.72	97
4	41	0.13	18.15	2.64	5.42	204
Avg	**48**	**0.15**	**18.70**	**2.28**	**4.02**	**149**
St Dev	**10**	**0.03**	**6.98**	**0.40**	**0.97**	**45**

Table 3

Water mass loss (%) for hydrated and dehydrated silk film samples for different processing conditions.

Sample	Water-annealed		MeOH Immersion	
	Hydrated	Dehydrated	Hydrated	Dehydrated
1	49	7	77	10
2	36	8	85	7
3	39	8	76	6
Avg	**41.3**	**7.7**	**79.3**	**7.7**
St Dev	**6.8**	**0.6**	**4.9**	**2.1**

Table 4

The 1st derivative peak positions calculated from the TGA mass loss profiles of hydrated and dehydrated silk film samples from different processing conditions.

Sample	Water-Annealed			MeOH Immersion		
	Hydrated		Dehydrated	Hydrated		Dehydrated
	1st Peak	2nd Peak		1st Peak	2nd Peak	
1	24.1	276.0	276.0	76.0	276.5	280.0
2	NA	270.0	275.0	52.5	275.0	279.0
3	NA	271.6	274.8	52.8	270.0	278.0
Avg	**24.1**	**272.5**	**275.3**	**60.4**	**273.8**	**279.0**
St Dev	**NA**	**3.1**	**0.6**	**13.5**	**3.4**	**1.0**

Table 5

Silk film thickness and oxygen permeability properties for multiple processing and RH conditions.

Testing Condition	FilmThickness (μm)	O_2GTR (mL O_2/m^2·d)		Dk [10^{-11}(mL O_2·cm)/(s·cm^2·mmHg)]		Time to Steady State (min)
		15 (min)	135 (min)	15 (min)	135 (min)	
Water-annealed @ 80% RH	29.6 ± 6.3	4,143 ± 1,953	4,245 ± 1,989	1.75 ± 0.43	1.80 ± 0.41	65 ± 8.66
MeOH treated @ 80% RH	95.7 ± 2.4	2,971 ± 91	3,701 ± 61	4.07 ± 1.50	5.07 ± 1.44	> 135
Water-annealed @ 50% RH	40.5 ± 9.7	375.0 ± 54.7	54.7 ± 25.7	0.21 ± 0.05	0	50 ± 8.66
MeOH treated @ 50% RH	89.1 ± 1.4	1,655 ± 704	185 ± 104	2.25 ± 0.98	0.25 ± 0.14	> 135

RH – relative humidity; O_2GTR – oxygen transmissibility; Dk – oxygen permeability coefficient (n=3, error=SD)